ARTICLE NO. 80-4046

Pursuit-Evasion of Two Aircraft in a Horizontal Plane

N. Rajan,* U.R. Prasad,† and N.J. Rao‡
Indian Institute of Science, Bangalore, India

Pursuit-evasion between two aircraft in a horizontal plane is analyzed as a differential game using point-mass aircraft models. A suitable choice of real-space coordinates confers open-loop optimality on the game. The solution in the small is described in terms of the individual aircraft's extremal trajectory maps (ETM). Each is independent of role, adversary, and capture radius. An ETM depicts the actual trajectories flown by the aircraft in real space. A template method of generating constant control arcs is described. This is used to investigate bank saturation and throttle switching behavior exhaustively. Sections of the barrier are obtained by iteratively choosing pairs of extremals from the two ETM's.

I. Introduction

ANALYTICAL studies of aircraft pursuit-evasion techniques seek to determine the influence of aircraft and weapon system performance upon combat outcome and to derive idealized tactics. Aircraft pursuit-evasion is considerably more difficult to analyze than optimal maneuvers because a closed-loop solution is a must in a differential game situation and exceptional and discontinuous surfaces are the rule rather than an exception.

Analyses of aircraft pursuit-evasion have simplified the situation along three lines. First, pursuit-evasion has been studied as variants of the Game of Two Cars.[1-7] In these, the aircraft are assumed to fly at constant altitude and speeds; their optimal paths are composed of circular arcs and straight line segments. Second, in the energy approach,[8-11] the aircraft are modeled realistically in terms of their energies and relative heading. However, the relative positions of the aircraft are ignored. The differential game studied is again trimensional. Third, in the dynamic modeling[12] and numerical approaches,[13-16] combat is formulated as a game of prescribed duration thus avoiding discontinuous and exceptional surfaces. Even then, near-optimal closed-loop solutions have only been obtained for simple examples.[16] Thus an analysis of constant-altitude pursuit-evasion with varying aircraft speeds portrays the situation realistically. It also takes on, for the first time, a free-time combat game with five state variables.

The game is formulated in a real space whose origin and axes change from party to party. The equations decompose into two sets, one for each aircraft. These are coupled in terms of the terminal quantities alone. This simplifies the solution in the small and effects significant computational economy. Moreover, each aircraft's optimal motion in real space can be described in terms of an extremal trajectory map (ETM) which is independent of the adversary and of role. The ETM thus serves as a measure of an individual aircraft's combat performance.

Received Oct. 5, 1976; revision received Oct. 9, 1979.

Index categories: Military Missions; Performance; Guidance and Control.

*Graduate Student, School of Automation; presently, Engineer, ISRO Satellite Centre, Bangalore.

†Assistant Professor, Dept. of Aeronautical Engineering and School of Automation; on leave as Nuffield Fellow, School of Electronic System Design, Cranfield Institute of Technology, Cranfield, United Kingdom. Member AIAA.

‡Assistant Professor, School of Automation.

The barrier and switching surfaces (solution in the large) for the game are constructed by combining the two aircraft ETM's. This is illustrated by the computation of barrier sections (BS).

II. Differential Game Analysis

A. Formulation

Two aircraft pursuit-evasion in a horizontal plane is formulated here in real-space.§ In a Cartesian coordinate system (CCS) (whose origin and orientation are as yet arbitrary), the position and velocity vectors of the pursuer (P) and evader (E) are (x_i, y_i) and (M_i, β_i) for $i=1,2$, respectively, satisfy

$$\dot{x}_i = M_i \cos\beta_i \tag{1}$$

$$\dot{y}_i = M_i \sin\beta_i \tag{2}$$

$$\dot{M}_i = A_i(M_i)\pi_i - B_i(M_i) - C_i(M_i)\omega_i^2 \tag{3}$$

$$\dot{\beta}_i = \omega_i a_i(M_i)/M_i \tag{4}$$

Equations (3) and (4) are obtained by modeling the supersonic aircraft as point masses executing coordinated turns at constant altitude under the assumptions that 1) the change in mass is negligible, 2) the thrust vector is aligned with the zero-lift axis, 3) the cosine of angle of attack is near unity, and 4) the normal component of thrust is negligible in comparison to the lift (see Appendix A).

Each aircraft can vary its Mach number between the stall limit and the maximum velocity placard limit,

$$\underline{M}_i \le M_i \le \bar{M}_i \tag{5}$$

The throttle and bank controls (π_i, ω_i) are constrained as

$$0 \le \pi_i \le 1 \tag{6}$$

$$|\omega_i| \le 1 \tag{7}$$

Capture is said to occur when the distance between the aircraft is R and is shrinking. The payoff is the time to capture.

The variational Hamiltonian can be written as

$$H = \lambda_0 + \sum_{i=1}^{2} [\lambda_{x_i}\dot{x}_i + \lambda_{y_i}\dot{y}_i(\lambda_{M_i} + \mu_i)\dot{M}_i + \lambda_{\beta_i}\dot{\beta}_i] \tag{8}$$

where $\lambda_0 = 0$ for the Game of Kind and 1 for the Game of Degree.

§One of the reviewers suggested this simplified derivation starting from a real-space formulation. This is gratefully acknowledged.

In Eq. (8), μ_i adjoin $\dot{M}_i$ to H to account for the first-order state constraints of Eq. (5).[17] The μ_i satisfy the Kuhn-Tucker conditions

$$(-1)^i\mu_i\begin{cases} >0 & \text{if } M_i=\underline{M}_i \\ =0 & \text{if } \underline{M}_i<M_i<\bar{M}_i \\ <0 & \text{if } M_i=\bar{M}_i \end{cases} \tag{9}$$

The adjoint equations and transverstality condition can be written readily. The real-space coordinate system is chosen so that its origin coincides with the pursuer's terminal position and the x-axis is along the terminal line of sight (PE). This is possible because the game is invariant with respect to translation and rotation of the real-space coordinate system. The position and orientation adjoints integrate to

$$(-1)^i\lambda_{x_i}=\lambda_{x_{2f}} \tag{10}$$

$$\lambda_{y_i}=0 \tag{11}$$

$$\lambda_{\beta_i}=\lambda_{x_i}y_i\,(i=1,2) \tag{12}$$

Furthermore,

$$\lambda_{x_{2f}}=\begin{cases} 1 & \text{Game of Kind} \\ 1/(\dot{x}_{1f}-\dot{x}_{2f}) & \text{Game of Degree} \end{cases} \tag{13}$$

is always positive. This leads to a decoupling of the canonical equations of the game into two disparate, identical sets, one for each aircraft.

B. Derivation of Optimal Strategies

The optimal controls (π_i,ω_i), $i=1,2$ yield a saddle point for H. As H does not involve time explicitly, a first integral of motion is given by

$$\min_{(\pi_1,\omega_1)}\ \max_{(\pi_2,\omega_2)} H=0 \tag{14}$$

Using the normalized speed adjoints P_{M_i} and multipliers $\bar{\mu}_i$,

$$p_{M_i}\triangleq(-1)^{i+1}\lambda_{M_i}/\lambda_{x_{2f}} \tag{15}$$

$$\bar{\mu}_i\triangleq(-1)^{i+1}\mu_i/\lambda_{x_{2f}} \tag{16}$$

and integrating Eq. (12) into Eq. (8), Eq. (14) becomes

$$\lambda_0+\lambda_{x_{2f}}\left[\min_{(\pi_1,\omega_1)} H_1-\min_{(\pi_2,\omega_2)} H_2\right]=0 \tag{17}$$

since $\lambda_{x_{2f}}$ is positive definite. In Eq. (17),

$$H_i=(p_{M_i}+\bar{\mu}_i)\dot{M}_i-y_i\dot{\beta}_i-\dot{x}_i \qquad (i=1,2) \tag{18}$$

The constraints of Eqs. (6) and (7) on $(\pi_i,\ \omega_i)$, $i=1,2$ are also separable and identical in form. The optimal controls are

$$\pi_i=\text{stp}[-(p_{M_i}+\bar{\mu}_i)] \tag{19}$$

$$\omega_i=\begin{cases} \text{sat}[-a_iy_i/2C_iM_i(p_{M_i}+\bar{\mu}_i)] & \text{if } (p_{M_i}+\bar{\mu}_i)<0 \\ \text{sgn}(y_i) \quad \text{if } (p_{M_i}+\bar{\mu}_i)\geq 0 & (i=1,2) \end{cases} \tag{20}$$

where stp, sat, and sgn denote the step, saturation, and relay functions, respectively. Each aircraft's controls depend on its own normalized speed adjoint and multiplier as a consequence of the location and orientation of the CCS. The normalized speed adjoints of the aircraft satisfy, for $i=1,2$, the equation

$$\dot{p}_{M_i}=\cos\beta_i+y_i\mathrm{d}\dot{\beta}_i/\mathrm{d}M_i-p_{M_i}\mathrm{d}\dot{M}_i/\mathrm{d}M_i \tag{21}$$

(see Appendix B.)

Since the canonical equations (1-4) and (21) together with the controls [Eqs. (19 and (20)] form two disparate sets, one for each player, an "open-loop optimality" similar to that obtained in differential turns[10] is conferred here. Assume that the evader also ends at the origin of the CCS. Then its motion is described by the same equations as the pursuer's. The evader's new path need only be translated along the x-axis by the capture radius to give the actual path. If roles are reversed, aircraft 1's (the erstwhile pursuer) path is the one that is displaced by the capture radius. Thus a map of the paths emanating from the origin for different values of (M_{if},β_{if}) represents the behavior of the aircraft as pursuer and evader. This map is termed an extremal trajectory map (ETM) and the solution in the small is discussed in terms of the ETM's.

Remark: The position and orientation of the CCS change from party to party (fixed only when the termination is known). Thus (x_i,y_i) can be calculated only in retro time $\tau(=t_f-t)$. The relation between the reduced space quantities r, ψ_i, $i=1,2$ and the CCS quantities is evident from Fig. 1. While constructing a reduced space trajectory from a pair of extremals, it can be easily checked that r increases in retro time.

III. Construction of an Aircraft ETM

A. Types of Extremals

The normalized speed adjoint can be integrated analytically. This simplifies the derivation of extremals and the study of switching behavior. The numerical values for the example aircraft (both of which are assumed identical) are taken from Ref. 18. The stall angle of attack is taken as 12 deg.

For $\dot{M}_i\neq 0$, Eq. (21) can be multiplied by $\dot{M}_i$ and integrated by parts between any t and t_f to give

$$\dot{M}_ip_{M_i}=M_i\cos\beta_i-M_{if}\cos\beta_{if}+y_i\dot{\beta}_i \tag{22}$$

which reduces Eq. (18) to $H_i=-M_{if}\cos\beta_{if}$.

If $\dot{M}_i=0$ for a full bank arc, the Mach number will be constant over a finite time interval and p_{M_i} can be integrated analytically. This can happen only at $M_i=M^*$ which is 0.75 for the example aircraft. On a partial bank arc, the vanishing

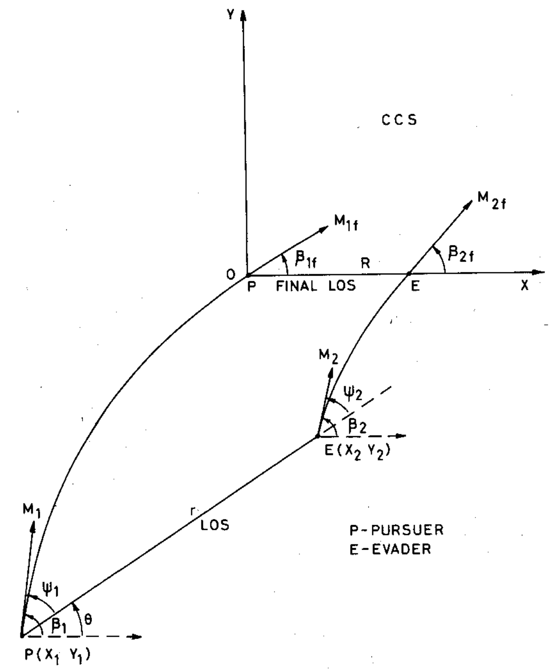

Fig. 1 Relation between reduced space and Cartesian coordinate system.

of $\dot{M}_i$ requires that

$$|\omega_i| = [(A_i - B_i)/C_i]^{1/2} < 1 \tag{23}$$

Since $A_i - B_i > C_i$ below M^*, $\dot{M}_i \neq 0$ there. Numerical experience shows that $\dot{M}_i$ vanishes instantaneously only above M^*.

From Eqs. (19) and (20) it is clear that the control combination of zero throttle and partial bank is nonoptimal. Full throttle partial bank, full throttle full bank, and zero throttle full bank are the optimal nonsingular control combinations.

Singular values of π_i may be optimal if M_i is within bounds and $p_{M_i} \equiv 0$. Equating successive time derivatives of p_{M_i} to zero gives

$$\cos\beta_i + |y_i| M_i^{-1} (\mathrm{d}a_i/\mathrm{d}M_i - a_i M_i^{-1}) = 0 \tag{24}$$

$$\omega_i \sin\beta_i (\mathrm{d}a_i/\mathrm{d}M_i - 2a_i M_i^{-1}) + \dot{M}_i M_i^{-1} |y_i| (\mathrm{d}^2 a_i/\mathrm{d}M_i^2 - 2M_i^{-1} \mathrm{d}a_i/\mathrm{d}M_i + 2a_i M_i^{-2}) = 0 \tag{25}$$

In Eq. (25), ω_i is given by the relay function in Eq. (20). Hence Eq. (25) gives $\dot{M}_i$ and π_i. The π_i so obtained must satisfy the Generalized Legendre Clebsch condition.[17]

$$\mathrm{d}^2 a_i/\mathrm{d}M_i^2 - 2M_i^{-1} \mathrm{d}a_i/\mathrm{d}M_i + 2aM_i^{-2} \leq 0 \tag{26}$$

For $M_i > \hat{M}$, the Mach number corresponding to the corner velocity, the acceleration limit $a_i(M_i)$ is set by pilot tolerance and is constant; hence Eq. (26) is violated. Below $\hat{M}$, it is lift limited. Here, no optimal paths terminate as singular throttle arcs. However, it is possible that the normalized speed adjoint and its time derivatives vanish at the retro throttle switching instant τ_s. The extremal then continues as a singular arc along which Eqs. (22) and (24) combine to yield

$$|y_i| (\mathrm{d}a_i/\mathrm{d}M_i - 2a_i M_i^{-1}) = -M_{if} \cos\beta_{if} \tag{27}$$

The singular arc will continue as long as π_i calculated from Eqs. (27) and (25) remains within $|0,1|$.

A possibility of chattering arises if in Eq. (18), $y_i \equiv 0$ and $p_{M_i} > 0$. It turns out that such a chattering arc does not satisfy the Kelley-Contensou test for optimality.

An extremal trajectory may consist of a segment on the upper or lower speed bounds joining an unconstrained arc. However, only straight line dashes along the negative x-axis satisfy the necessary junction condition (see Appendix C).

At termination, the quantities p_{M_i} and y_i appearing in Eqs. (19) and (20) vanish. Thus the terminal strategies depend on the derivatives of these quantities and are given as

$$\pi_i = \mathrm{stp}(\cos\beta_{if}) \tag{28}$$

$$\omega_i = \begin{cases} \mathrm{sat}(-a_i \tan\beta_{if}/2C_i) & \text{if} \quad \cos\beta_{if} > 0 \\ -\mathrm{sgn}(\sin\beta_{if}) & \text{if} \quad \cos\beta_{if} \leq 0 \end{cases} \tag{29}$$

The angle at which the terminal bank in Eq. (29) saturates is

$$\beta_{l_i}(M_i) = \arctan[2C_i(M_i)/a_i(M_i)] \tag{30}$$

For $M_i = \bar{M}_i$, there are no retrogressive paths for

$$\beta_{if} > \beta_i^* = \arctan\{2[C_i(A_i - B_i)]^{1/2}/a_i\} \tag{31}$$

as the necessary condition of Eq. (9) is contravened. At the lower boundary $\underline{M}_i$, the turn rates are practically zero and the extremals are simply straight lines emanating at different β_{if}. For $|\beta_{if}| > 90$ deg, the extremals terminate with $\pi_i = 0$ and $|\omega_i| = 1$.

Thus it is noted that the terms of extremals obtained are full bank arcs with the throttle closed or open and partial bank arcs with the throttle open. The former are constant control arcs (CCA's) and can be generated without integration using trajectory templates.

B. Templates

A template is a path flown with throttle and bank controls held constant. The path is described in a coordinate system fixed in the plane with the origin coinciding with the initial position of the aircraft and the x-axis along the initial velocity vector. The trajectory templates for the given aircraft are shown in Fig. 2. All the curves are flown with $\omega = 1$. Curve 1 flown at full throttle accelerates from $\underline{M}$ to M^*. As the Mach number approaches $M^* = 0.75$, the acceleration tends to zero and the curve becomes circular. Curve 2 again flown at full throttle decelerates from $\bar{M}$ to M^*. The third curve is flown with zero throttle throughout and slows from $\bar{M}$ to $\underline{M}$. Points are marked on the template curves at 1-s intervals. The corresponding curves for negative bank are simply the mirror images of these three along the x-axis.

The CCA is described in a coordinate system fixed to the plane. It can thus be constructed without integration by translation and rotation of a template segment. This also permits a global investigation of control switching.

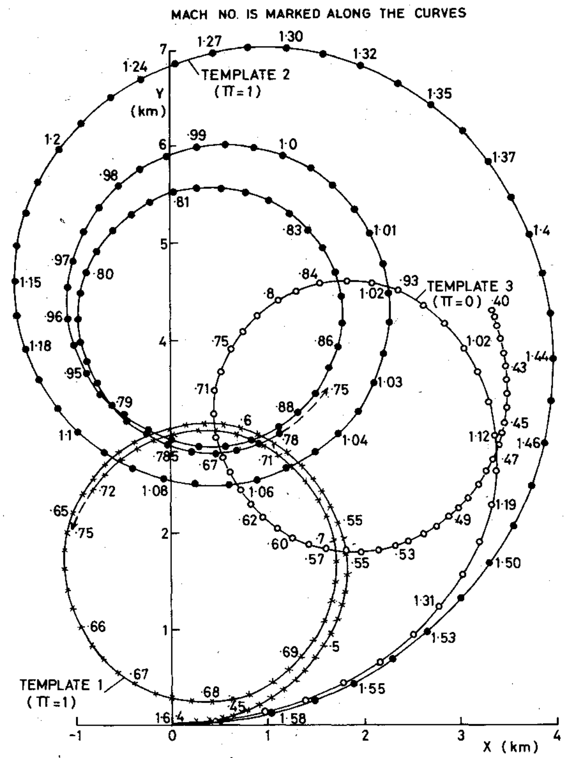

Fig. 2 Full bank aircraft trajectory templates.

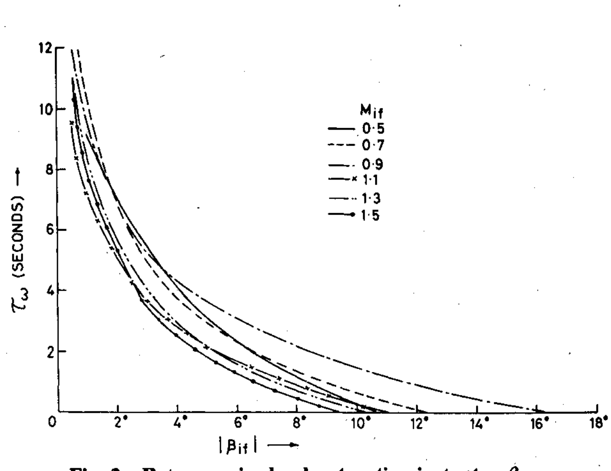

Fig. 3 Retrogressive bank saturation instant vs β_{if}.

C. Bank Saturation, Throttle, and Bank Switching

At termination ($\tau=0$), $\omega_i=0$ for $\beta_{if}=0$ from Eq. (29). As $|\beta_{if}|$ increases, $|\omega_i|$ increases until it becomes unity at $|\beta_{if}|=\beta_{li}$. Along extremals with a partial bank segment, the bank increases in retro time. For small $|\beta_{if}|$ the retrogressive path encounters the lower speed boundary before the bank saturates. For larger $|\beta_{if}|$ values, an implicit algebraic relation for the bank saturation instant τ_ω can be obtained by eliminating p_{M_i} between Eqs. (20) and (22). Plots of τ_ω vs β_{if} for different M_{if} are shown in Fig. 3.

From Eq. (19), throttle switches at the zeros of p_{M_i}. Thus Eq. (22) becomes an implicit relation for the throttle switching instants. Switching replaces one sort of CCA with another; all the quantities involved in the relation can be readily computed in terms of the template quantities. This greatly reduces the computation time required to determine the switching instant and permits extensive numerical investigation of throttle switching behavior.

Figure 4 shows the first throttle switching instant τ_{sl} (from one to zero) vs β_{if} for different M_{if}. For $M_{if}\leq 0.8$, there is no throttle switching when $|\beta_{if}|<90$ deg. This is justified because, in this Mach number range, turn rate improves with Mach number and there would be little point in decelerating. For the Mach number range plotted in Fig. 4, there is only a single switch in throttle from one to zero. For $M_{if}=1.5$ there is no switch in throttle for $|\beta_{if}|<40$ deg as the retrogressive paths stop once $M_i=\hat{M}$.

Figure 5 depicts the variation of the first throttle switching instant τ_{sl} from zero to one. At $\tau=0$, $\pi_i=0$ for $|\beta_{if}|>90$ deg from Eq. (28). Extremals with $M_{if}>\hat{M}$ continue backward in time with $\pi_i=0$ until they intersect the x-axis. There is a second switch in throttle (from one to zero) which appears at $|\beta_{if}|=94$ deg for $M_{if}=0.8$. This throttle closure occurs just after M_i crosses $\hat{M}$. The interval between the two switching instants decreases with increase in $|\beta_{if}|$ and eventually vanishes. Beyond this there is no switch in throttle before the extremal cuts the x-axis. Also, for $M_{if}=0.75$ and 0.7, the second switch in throttle occurs just after $\hat{M}$ is crossed, first appearing after $|\beta_{if}|=98$ and 100 deg, respectively. Extremals for $M_{if}=0.6$ and 0.5 do not show any second switch in throttle. There is a small range of $|\beta_{if}|=98.6$ and 98.9 deg for $M_{if}=0.6$ and 106.3 and 107.8 deg for $M_{if}=0.5$, over which singular throttle arcs arise (see Sec. III. A). These are at the end of the switching region. The junction times τ_j between the nonsingular and singular arcs are:

1) $M_{if}=0.6$, $|\beta_{if}|=98.6$ deg, $\tau_j=10.1$ s
   $|\beta_{if}|=98.9$ deg, $\tau_j=9.1$ s
2) $M_{if}=0.5$, $|\beta_{if}|=106.3$ deg, $\tau_j=12.1$ s
   $|\beta_{if}|=107.8$ deg, $\tau_j=9.1$ s

Beyond this the extremals cut the x-axis without switching throttle.

D. Extremal Trajectory Maps

The ETM's for $M_{if}=0.5$ and 1.3 are shown in Figs. 6 and 7, respectively. In the partial bank region, turn rate is exchanged for greater longitudinal acceleration. For $|\beta_{if}|>\beta_{l_i}$, all the extremals are CCA's with $\pi_i=0$ or 1. In the case of $M_{if}=1.3$, partial bank arcs decelerate (in retro time) below 1.3 and then accelerate.

From the above it is clear that the extremal for any (M_{if},β_{if}) can be traced in retro time. The solution of the game in the large determines for what values this need be done.

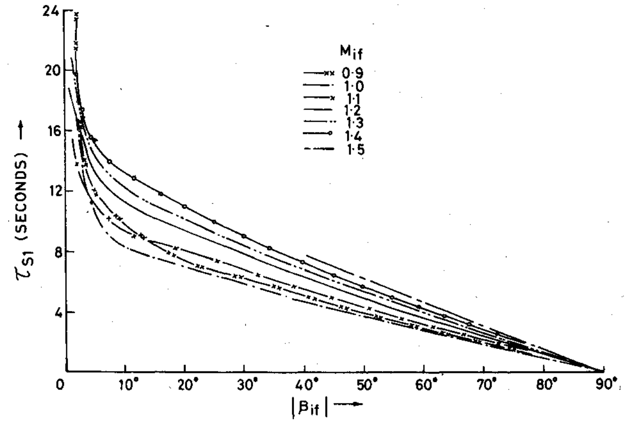

Fig. 4 First throttle switching instant ($\pi=1$ to $\pi=0$) vs β_{if}.

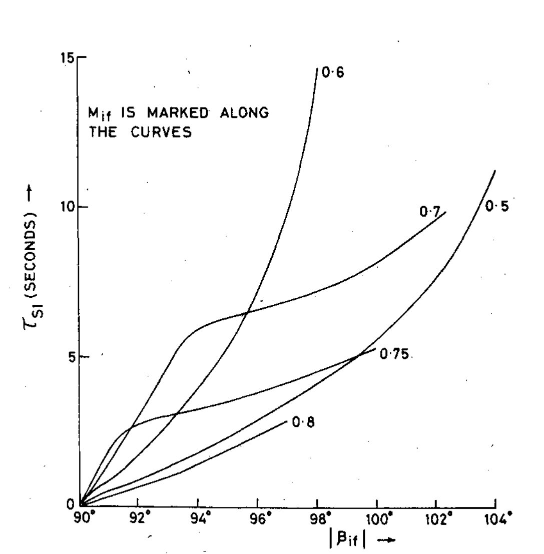

Fig. 5 First throttle switching instant ($\pi=0$ to $\pi=1$) vs β_{if}.

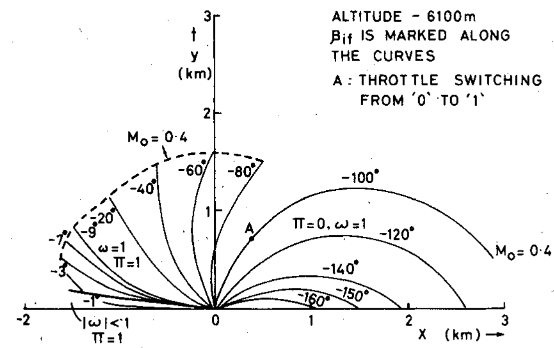

Fig. 6 Extremal trajectory map for $M_{if}=0.5$.

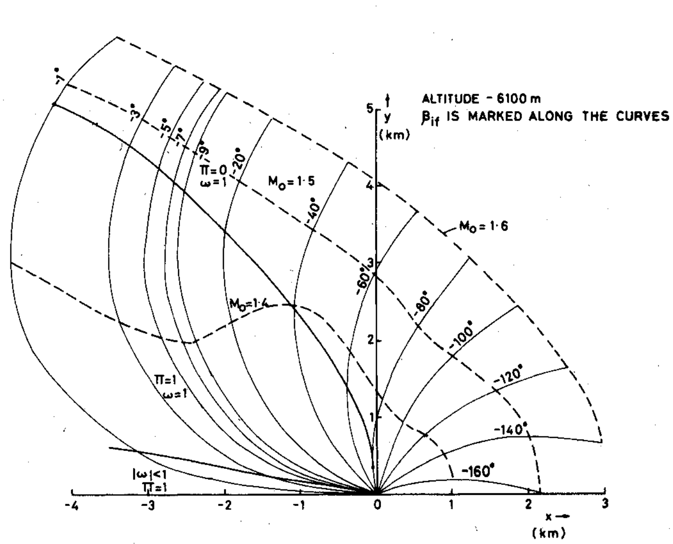

Fig. 7 Extremal trajectory map for $M_{if}=1.3$.

IV. Construction of the Barrier

A. Method of Approach

The barrier and switching surfaces for the game are hypersurfaces in the reduced space. For a given set of initial Mach numbers M_{10}, M_{20} and relative orientation β_0, the corresponding barrier section (BS), depending upon whether it is open or closed, delineates the relative evader positions that result in easy and involved/impossible capture. Thus barrier sections for different sets of M_{10}, M_{20}, β_0 depict the solution to the Game of Kind. So do the switching surface sections for the Game of Degree.

The BS for M_{10}, M_{20}, β_0 intersects all the retrogressive paths on which M_1, M_2, $\beta=(\beta_2-\beta_1)$ simultaneously attain M_{10}, M_{20}, β_0. It is noted that β_{1f} parameterizes the BS. As β_{2f} is obtained by the Boundary of the Usable Part (BUP) condition

$$\cos\beta_{2f}=M_{1f}\cos\beta_{1f}/M_{2f} \tag{32}$$

a two-dimensional search on M_{1f}, M_{2f} is required to match the speeds and relative orientation. In other words, for a given β_{1f}, a barrier path results for each choice of M_{1f}, M_{2f} bound by Eq. (32). At the instant τ_0 when β equals β_0 let the Mach numbers be M_{1a}, M_{2a}. The search for M_{1f}, M_{2f} to match speeds can be posed as the minimization of

$$F=w_1(M_{10}-M_{1a})^2+w_2(M_{20}-M_{2a})^2$$
$$(w_1, w_2=\text{weights}) \tag{33}$$

Furthermore, since the aircraft abscissas do not influence the other ETM variables, speeds and orientation can be matched without taking the capture radius and the choice of roles into account. Position coordinates can then be determined for any set of roles and capture radii even by hand computation. The above procedure can be easily modified to construct any of the switching surface sections. Here, the search for terminal velocity vectors further decomposes into a one-dimensional search for M_{1f} and a two-dimensional search for (M_{2f},β_{2f}).

The Powell search method has been used to minimize Eq. (33). Provision is made to reduce the step size whenever a violation of the constraints on M_{1f}, M_{2f} is imminent. Using the templates for all the CCA portions of the extremals (Sec. III. B) and for the calculation of switching instants (Sec. III. C) reduced the time taken to evaluate F to the order of milliseconds. Typically, 50 function evaluations were needed to minimize F for most points on the barrier sections. The overall saving in computation time was therefore tremendous.

B. Barrier Sections for an Initially Slower Pursuer

The BS for $M_{10}=0.9$, $M_{20}=1.2$ are shown in Fig. 8. Four encounters starting at different points on the BS are shown in Fig. 9. For the parties from positions E_1 and E_3 on the BS, the pursuer banks partially throughout to turn through 11 and 35 deg, respectively. The retrogressive paths corresponding to E_2 and E_4 last for about 4 s. For E_2 both aircraft employ zero throttle throughout. The party corresponding to E_4 has both aircraft switching throttle from zero to one, P almost immediately and E 2.4 s later. The encounter at the dispersal point (DP)D_1 is qualitatively similar to that for E_3; only P banks sharply at first before leveling out gradually. In all these cases, it is seen that E's deviation from the optimal strategy would result in its running into P, aiding capture. Similarly P's deviation would result in E's escape.

The barrier sections for other initial speeds are also of similar shape. The BS for $M_{10}=0.7$, $M_{20}=0.9$ of Fig. 10 shows that the capture zone shrinks quickly even with a modest reduction in P's initial speed.

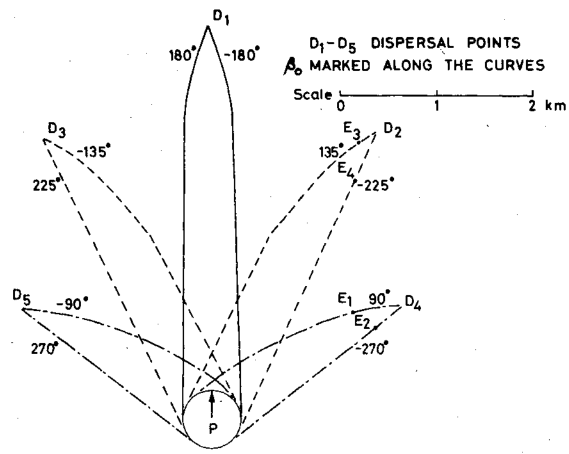

Fig. 8 Barrier sections in reduced space for $M_{10}=0.9, M_{20}=1.2$

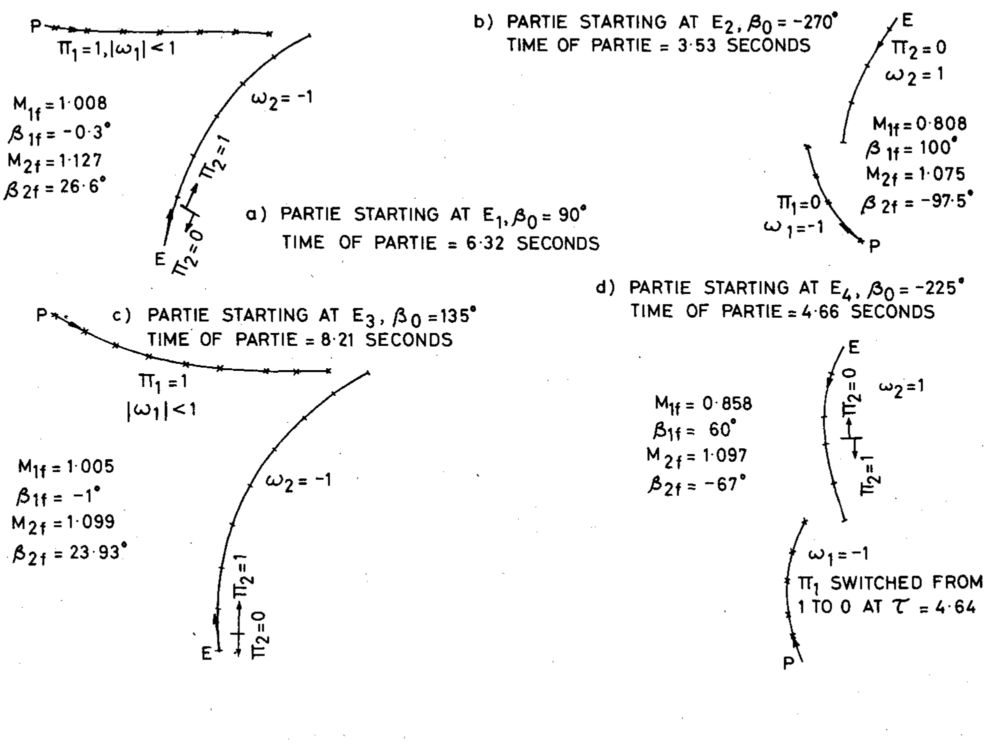

Fig. 9 Parties starting on BS(0.9, 1.2) shown in real space.

C. The Case of the Initially Faster Pursuer

The barrier sections should close even here, for a sufficiently distant E will be able to turn tail and accelerate to $\bar{M}$ before P can narrow the range to the capture radius.

The points obtained on a barrier section with $M_{10}=1.2$, $M_{20}=0.9$, $\beta_0=180$ deg are plotted in Fig. 11. These are obtained from the Mach number/orientation matches obtained for Fig. 8. The curves diverge from each other as P progressively turns more than E. At the head-on dispersal point, E has to turn through an angle far in excess of P in avoiding capture. Between the head-on dispersal point and the diverging curves obtained earlier, E turns less and less and P increasingly more. This portion of the barrier section intersects the diverging curves (on which P turns more than E) at a dispersal point where E has a choice between outturning or outpacing P in warding off capture. The attempt to obtain the barrier section between the two dispersal points ran into numerical difficulties because when β_{if} is very small ($i=1,2$), $M_{if}=\bar{M}$ and the aircraft extremal trajectories are very long.

Two methods are explored for solving the problem. The first is an approximate calculation in which E is assumed to turn at full throttle through a large angle (180 deg $-\delta$) and accelerate to $\bar{M}$. Meanwhile, P first turns through δ and then accelerates to $\bar{M}$ at full throttle. During the flight at a constant speed $\bar{M}$ that ensues, P just manages to close the range to R. Using this encounter geometry in conjunction with the full bank templates of Fig. 2 and the straight line template (accelerating from $\underline{M}$ to $\bar{M}$ in level flight), E's relative position on the barrier section can be determined for different δ. This is illustrated by the broken line in Fig. 11. The other method, called the extended Meier technique,[19] is based on the Envelope Principle of Isaacs. It is new in concept and is under development.

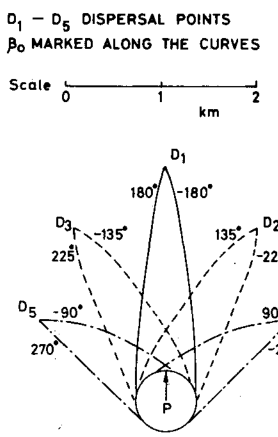

Fig. 10 Barrier sections in reduced space for $M_{10}=0.7$, $M_{20}=0.9$.

V. Conclusions

The formulation of the game in a suitably chosen real space coordinate system leads to a decoupling of the game equations into two independent sets. The solution in the small is discussed in terms of the aircraft extremal trajectory maps. The ETM contains the whole gamut of maneuvers that an aircraft may be called upon to perform in combat. It is the same whether the aircraft is pursuing or evading. Barrier and switching surfaces can be constructed by combining the two aircraft ETM's. Thus, if one aircraft is changed, only its ETM need be replaced.

In the solution in the large for the game, the matching of initial speeds and relative orientation is separated from the computation of the relative positions. Thus, once barrier sections are obtained for one value of the capture radius, those for other values and for the reversal of roles can be computed by hand. All these ideas are novel and result in phenomenal reduction in computation time. The ETM idea works for other generalizations of capture set geometry (e.g., fan shape) and dynamics (e.g., three-dimensional energy formulation that includes relative position information). Barrier sections for the game in which one aircraft flies at constant speed have also been determined.

Appendix A: Aircraft Model for Flight in a Horizontal Plane

Equations (3) and (4) are the usual acceleration and turn rate expressions for an aircraft in horizontal flight, only they are normalized here by the sonic speed c. The bank control is related to the actual bank σ and maximum permissible bank $\sigma_{\max}$ by $\omega=\tan\sigma/\tan\sigma_{\max}$. The functions A, B, C, and a are defined as

$$A(M)=T_{\max}(M)/mc \tag{A1}$$

$$B(M)=[D_0(M)+D_{L_0}(M)]/mc \tag{A2}$$

$$C(M)=D_{L_0}(M)\tan^2[\sigma_{\max}(M)]/mc \tag{A3}$$

$$a(M)=(g/c)\tan\sigma_{\max}(M) \tag{A4}$$

Here $D_0(M)$ and $D_{L_0}(M)$ are the base drag and lift induced drag at zero bank as in Ref. 18. The Mach number for which the maximum permissible turn rate $a(M)/M$ reaches a peak is the corner velocity $\hat{M}$.

Appendix B: Equation for Speed Adjoints

The normalized speed adjoints satisfy the differential equation

$$\dot{p}_{M_i}=(-1)^i(1/\lambda_{x_{2f}})\partial H/\partial M_i=\cos\beta_i+[y_i\omega_i \mathrm{d}f_i/\mathrm{d}M_i - (p_{M_i}+\bar{\mu}_i)(\pi_i \mathrm{d}A_i/\mathrm{d}M_i-\mathrm{d}B_i/\mathrm{d}M_i-\omega_i^2\mathrm{d}C_i/\mathrm{d}M_i)] \tag{B1}$$

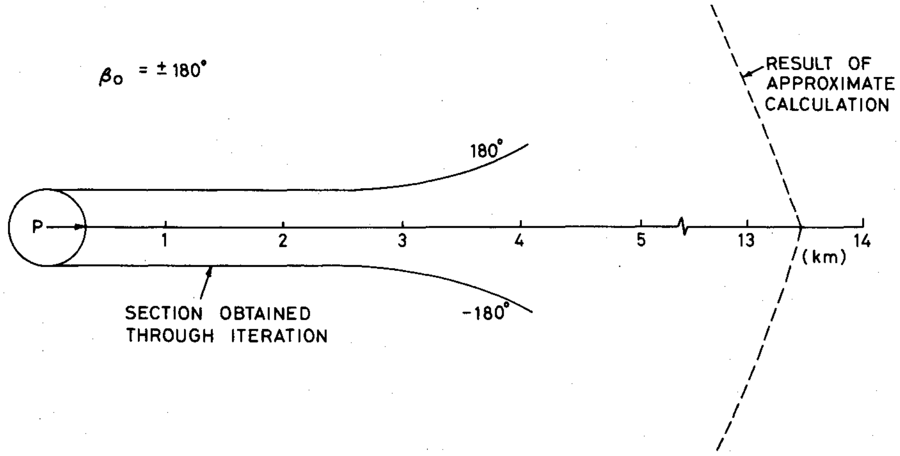

Fig. 11 Barrier sections in reduced space for $M_{10}=1.2$, $M_{20}=0.9$.

with $f_i = a_i/M_i$.

Where $\dot{M}_i \neq 0$, the speed is within bounds and $\bar{\mu}_i = 0$. Note that from Eqs. (4) and (3),

$$\mathrm{d}\dot{\beta}_i/\mathrm{d}M_i = \omega_i \mathrm{d}f_i/\mathrm{d}M_i + f_i \mathrm{d}\omega_i/\mathrm{d}M_i \tag{B2}$$

$$\mathrm{d}\dot{M}_i/\mathrm{d}M_i = \pi_i \mathrm{d}A_i/\mathrm{d}M_i - \mathrm{d}B_i/\mathrm{d}M_i - \omega_i^2 \mathrm{d}C_i/\mathrm{d}M_i$$
$$- 2C_i\omega_i \mathrm{d}\omega_i/\mathrm{d}M_i \tag{B3}$$

These expressions are multiplied by y_i and p_{M_i}, respectively, and Eq. (B3) is substracted from Eq. (B2) to give

$$y_i \mathrm{d}\dot{\beta}_i/\mathrm{d}M_i - p_{M_i}\mathrm{d}\dot{M}_i/\mathrm{d}M_i = y_i\omega_i \mathrm{d}f_i/\mathrm{d}M_i$$
$$- p_{M_i}(\pi_i \mathrm{d}A_i/\mathrm{d}M_i - \mathrm{d}B_i/\mathrm{d}M_i - \omega_i^2 \mathrm{d}C_i/\mathrm{d}M_i)$$
$$+ (y_i f_i + 2p_{M_i} C_i\omega_i)\mathrm{d}\omega_i/\mathrm{d}M_i \tag{B4}$$

For partial bank, $\partial H_i/\partial\omega_i = y_i f_i + 2p_{M_i} C_i \omega_i = 0$ and for full bank, $\mathrm{d}\omega_i/\mathrm{d}M_i = 0$. Thus the left side of Eq. (B4) can replace the term within square parentheses in Eq. (B1) giving Eq. (21).

Appendix C: Boundary Arcs

As the state constraints of Eq. (5) involve only the speed, the speed adjoint alone is discontinuous at the junction point where the extremal reaches a speed boundary.[17] Since $\dot{M}_i^+ = 0$ (the '+' refers to the constrained arc), the continuity of H implies

$$a_i y_i(\omega_i^- - \omega_i^+)/M_i = p_{M_i}^- \dot{M}_i^- \tag{C1}$$

Straight line dashes along the negative x-axis satisfy Eq. (C1) identically since $p_{M_i}^- = 0$ from Eq. (21).

As the example aircraft decelerates on full bank full throttle arcs for speeds above M^*, a retrogressive path may meet the upper speed boundary with either zero throttle or full throttle. The optimality of these extremals is tested by checking Eq. (C1) with Eqs. (19) and (20) applied on both sides of the junction. For example, assuming that M_i reaches $\bar{M}_i$ with $\pi_i^- = 0$, then $p_{M_i}^- > 0$ from Eq. (19), making the right side of Eq. (C1) negative. But on the constrained arc, $\dot{M}_i^+ = 0$ precludes full bank. From Eqs. (19) and (20) it follows that

$$\pi_i^+ = 1 \quad \omega_i^+ = [(A_i - B_i)/C_i]^{1/2}\mathrm{sgn}(y_i) \quad \omega_i^- = \mathrm{sgn}(y_i)$$

These make the left side of Eq. (C1) positive which is a contradiction.

Similar analysis for other curved extremals shows that Eq. (C1) is violated and the extremals stop once they reach either speed boundary.

Acknowledgments

The assistance of S. Ramgopal in obtaining the numerical results is gratefully acknowledged.

References

[1]Isaacs, R., *Differential Games*, John Wiley & Sons, New York, 1965.

[2]Breakwell, J.V. and Merz, A.W., "Minimum Required Capture Radius in a Coplanar Model of the Aerial Combat Problem," *AIAA Journal*, Vol. 15, Aug. 1977, pp. 1089-1094.

[3]Lynch, U.H.D., "Differential Game Barriers and Their Application in Air-to-Air Combat," Ph.D. Dissertation, DS/MC/73-1, Air Force Institute of Technology, Wright-Patterson Air Force Base, Ohio, March 1973.

[4]Merz, A.W., "The Game of Two Identical Cars," *Multicriteria Decision Making and Differential Games*, edited by G. Leitmann, Plenum Press, New York, 1976, pp. 421-442.

[5]Kelley, H.J. and Lefton, L., "Estimation of Weapon-Radius vs Maneuverability Tradeoff for Air-to-Air Combat," *AIAA Journal*, Vol. 15, Feb. 1977, pp. 145-148.

[6]Peng, W.Y. and Vincent, T.L., "Some Aspects of Aerial Combat," *AIAA Journal*, Vol. 13, Jan. 1975, pp. 7-11.

[7]Merz, A.W. and Hague, D.S., "Coplanar Tail-Chase Aerial Combat as a Differential Game," *AIAA Journal*, Vol. 15, Oct. 1977, pp. 1419-1424.

[8]Kelley, H.J. and Lefton, L., "Differential Turns," *AIAA Journal*, Vol. 11, June 1973, pp. 858-861.

[9]Kelley, H.J., "Differential Turning Optimality Criteria," *Journal of Aircraft*, Vol. 12, Jan. 1975, pp. 41-44.

[10]Kelley, H.J., "Differential Turning Tactics," *Journal of Aircraft*, Vol. 12, Dec. 1975, pp. 930-966.

[11]Kelley, H.J. and Lefton, L., "Calculation of Differential-Turning Barrier Surfaces," *Journal of Spacecraft and Rockets*, Vol. 14, Feb. 1977, pp. 87-95.

[12]Anderson, G.M., Othling, W.L., and Williamson-Noble, S.M.D., "The Dynamic Modelling Technique for Obtaining Closed-Loop Control Laws for Aircraft/Aircraft Pursuit-Evasion Problems," *Proceedings of the Joint Automatic Control Conference*, Stanford University, Aug. 16-18, 1972, pp. 953-954.

[13]Roberts, D.A. and Montgomery, R.C., "Development and Application of a Gradient Method for Solving Differential Games," NASA TND-6502, Nov. 1971.

[14]Leatham, A.L. and Lynch, U.H.D., "Two Numerical Methods to Solve Realistic Air-to-Air Combat Differential Games," AIAA Paper 74-22, Washington D.C., Feb. 1974.

[15]Anderson, G.M., "A Near-Optimal Closed-Loop Solution Method for Nonsingular Zero-sum Differential Games," *Journal of Optimization Theory and Applications*, Vol. 13, No. 3, 1974, pp. 303-318.

[16]Jarmark, B.S.A., "Near-Optimal Closed-Loop Strategy for Aerial Combat Games," Dept. of Automatic Control, The Royal Institute of Technology, Stockholm, Sweden, TRITA-REG-7602, March 1976.

[17]Bryson, A.E., Jr., and Ho, Y.C., *Applied Optimal Control*, Blaisdell Publishing Co., Waltham, Mass., 1969, pp. 117-126.

[18]Bryson, A.E., Jr., and Parsons, M.G., "Constant Altitude Minimum-Time Turns to a Line and to a Point for a Supersonic Aircraft with a Constraint on Maximum Velocity," Stanford University, SUDAAR No. 437, Nov. 1971.

[19]Rajan, N., "Differential Game Analysis of Two Aircraft Pursuit-Evasion," Ph.D. Dissertation, School of Automation, Indian Institute of Science, Bangalore, July 1978.